DOI: 10.1002/chem.201200809

From *lin*-Benzoguanines to *lin*-Benzohypoxanthines as Ligands for *Zymomonas mobilis* tRNA–Guanine Transglycosylase: Replacement of Protein–Ligand Hydrogen Bonding by Importing Water Clusters

Luzi Jakob Barandun,[a] Florian Immekus,[b] Philipp C. Kohler,[a] Sandro Tonazzi,[a] Björn Wagner,[c] Severin Wendelspiess,[c] Tina Ritschel,[b, d] Andreas Heine,[b] Manfred Kansy,[c] Gerhard Klebe,*[b] and François Diederich*[a]

Dedicated to Prof. Dr. Heribert Offermanns on the occasion of his 75th birthday

Abstract: The foodborne illness shigellosis is caused by *Shigella* bacteria that secrete the highly cytotoxic *Shiga* toxin, which is also formed by the closely related enterohemorrhagic *Escherichia coli* (EHEC). It has been shown that tRNA–guanine transglycosylase (TGT) is essential for the pathogenicity of *Shigella flexneri*. Herein, the molecular recognition properties of a guanine binding pocket in *Zymomonas mobilis* TGT are investigated with a series of *lin*-benzohypoxanthine- and *lin*-benzoguanine-based inhibitors that bear substituents to occupy either the ribose-33 or the ribose-34 pocket. The three inhibitor scaffolds differ by the substituent at C(6) being H, NH_2, or NH–alkyl. These differences lead to major changes in the inhibition constants, pK_a values, and binding modes. Compared to the *lin*-benzoguanines, with an exocyclic NH_2 at C(6), the *lin*-benzohypoxanthines without an exocyclic NH_2 group have a weaker affinity as several ionic protein–ligand hydrogen bonds are lost. X-ray cocrystal structure analysis reveals that a new water cluster is imported into the space vacated by the lacking NH_2 group and by a conformational shift of the side chain of catalytic Asp102. In the presence of an N-alkyl group at C(6) in *lin*-benzoguanine ligands, this water cluster is largely maintained but replacement of one of the water molecules in the cluster leads to a substantial loss in binding affinity. This study provides new insight into the role of water clusters at enzyme active sites and their challenging substitution by ligand parts, a topic of general interest in contemporary structure-based drug design.

Keywords: drug design · hydrogen bonds · molecular recognition · shigellosis · water clusters

Introduction

In May 2011, the outbreak of the *Shiga*-toxin-producing bacterium enterohemorrhagic *Escherichia coli* (EHEC) led to a major health and economic problem in Europe.[1] The eponymous bacterium for the *Shiga* toxin—the *Shigella* bacterium—causes the acute inflammatory bowel disease shigellosis.[2] It has been shown that the enzyme tRNA–guanine transglycosylase (TGT, EC 2.4.2.29) is a potential drug target for the treatment of shigellosis.[3,4] We have introduced 6-aminoimidazo[4,5-*g*]quinazolin-8(7*H*)-ones (*lin*-benzoguanines, Figure 1) as inhibitors of *Zymomonas mobilis* TGT.[5,6] The tricyclic, unsubstituted *lin*-benzopurines, in which the natural purine is extended by insertion of a benzene ring between the pyrimidine and the imidazole moieties, were introduced first by Leonard and co-workers in the 1970s.[7] They have, however, found only limited application in medicinal chemistry.[8–10] Kool and co-workers reported the synthesis and base-pairing properties of these extended nucleobases when introduced into oligonucleotides.[11]

In our previous studies on *Z. mobilis* TGT, we showed that highly potent inhibitors are obtained by filling either the ribose-33[12] or ribose-34 pocket[13,14] of the tRNA-binding site with substituents attached to C(2) or C(4), respec-

[a] L. J. Barandun,[+] Dr. P. C. Kohler, S. Tonazzi, Prof. Dr. F. Diederich
Laboratorium für Organische Chemie, ETH Zürich
Hönggerberg, HCI, 8093 Zurich (Switzerland)
Fax: (+41) 44-632-1109
E-mail: diederich@org.chem.ethz.ch

[b] F. Immekus,[+] Dr. T. Ritschel, Dr. A. Heine, Prof. Dr. G. Klebe
Institut für Pharmazeutische Chemie
Philipps-Universität Marburg, Marbacher Weg 6
35032 Marburg (Germany)
Fax: (+49) 6421-282-8994
E-mail: klebe@mailer.uni-marburg.de

[c] B. Wagner, S. Wendelspiess, Dr. M. Kansy
Pharma Research Non-Clinical Safety
F. Hoffmann-La Roche AG
4070 Basel (Switzerland)

[d] Dr. T. Ritschel
Current address: Computational Drug Discovery Group
CMBI, Radboud University Nijmegen Medical Centre
P.O. Box 9101, 6500 HB Nijmegen (The Netherlands)

[+] These authors contributed equally to this work.

Supporting information for this article is available on the WWW under http://dx.doi.org/10.1002/chem.201200809.

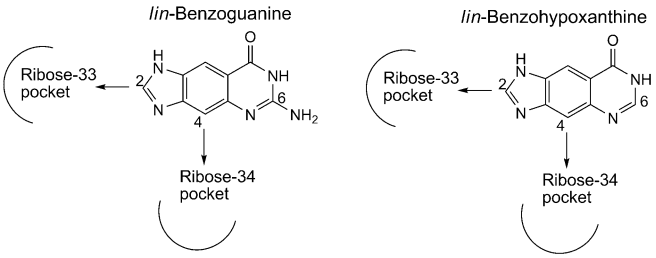

Figure 1. Structure and numbering of *lin*-benzoguanines and *lin*-benzohypoxanthines. Substitution at C(2) or C(4) allows the ribose-33 and ribose-34 pockets, respectively, to be filled.

tively, of the *lin*-benzoguanine core (Figure 1). Herein, we compare *lin*-benzoguanines with *lin*-benzohypoxanthines (imidazo[4,5-*g*]quinazolin-8(7*H*)-ones), which lack the exocyclic NH_2 group at C(6). Several comparative studies on the binding affinity of guanine and their corresponding hypoxanthine derivatives have been reported. Both cases are found in which either the guanine-based compounds have stronger binding than the hypoxanthine-based ones, or vice versa.[15,16] On the other hand, 9-deazahypoxanthine- and 9-deazaguanine-based ligands of the human purine nucleoside phosphorylase (PNP) were found to be equipotent.[17] These findings prompted us to investigate and compare the molecular recognition of *lin*-benzoguanines and *lin*-benzohypoxanthines by *Z. mobilis* TGT in detail.

Results and Discussion

Ligand design: *Z. mobilis* TGT catalyzes the guanine/preQ$_1$ base-exchange reaction at the wobble position G_{34} in the anticodon of bound tRNA with participation of the side chains of catalytic Asp102 and Asp280.[18] The region of the active site of interest for our ligand design comprises the guanine/preQ$_1$ binding pocket and the ribose-33 and ribose-34 pockets occupied by bound tRNA (Figure 2a). *lin*-Benzoguanines bound to the nucleobase pocket are intercalated between

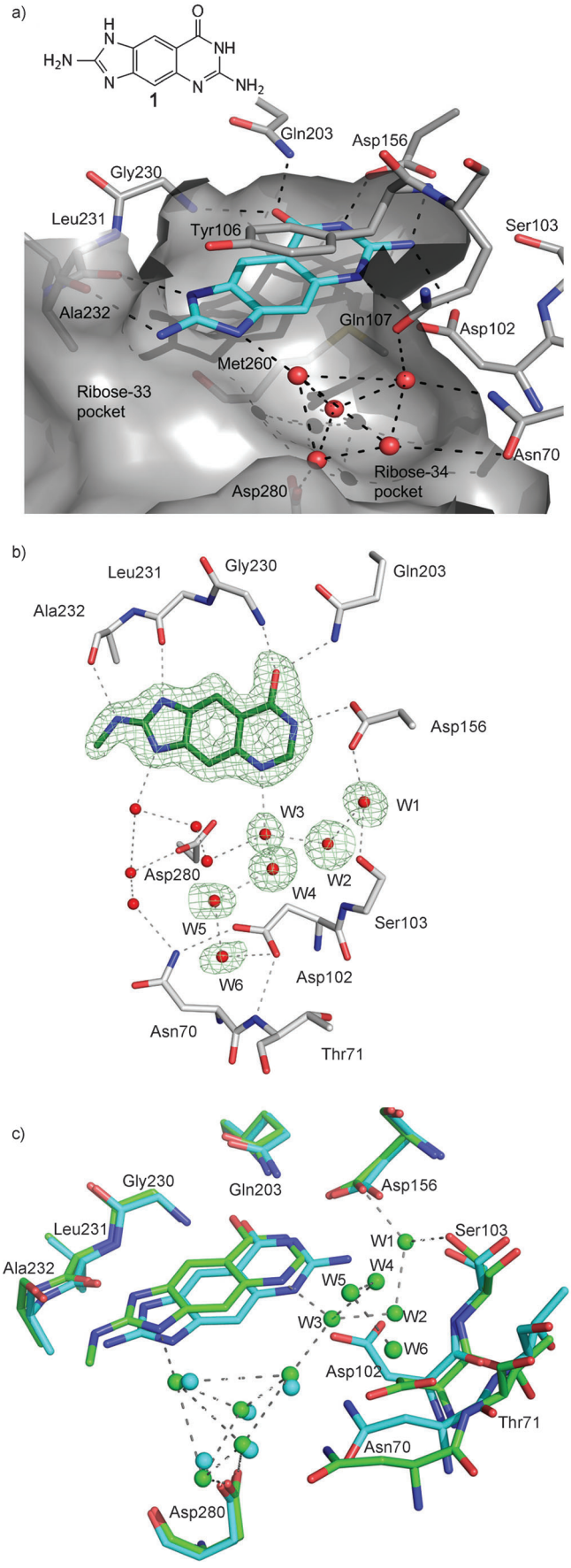

Figure 2. Comparison of X-ray cocrystal structures of *lin*-benzoguanines and *lin*-benzohypoxanthines bound to the active site of *Z. mobilis* TGT. Color code: C_{enzyme} gray, O red, N blue. Selected water molecules are shown as spheres and labeled as W (for residue identifiers, see Table 2SI in the Supporting Information). Hydrogen bonds are shown as dashed lines (distances between 2.5 and 3.5 Å). Ligand and water molecules are well defined by the difference electron density at 3σ shown as green mesh. These characteristics apply to all figure captions unless otherwise stated. a) Binding mode of *lin*-benzoguanine **1** (C_{ligand} cyan) in the active site of TGT (PDB code: 2Z7K[21]), which is indicated as a gray surface. The water cluster between Asp102 and Asp280 is shown as red spheres. b) Cocrystal structure of **8a** (C_{ligand} green) bound to the active site of TGT (PDB code: 3S1G). A hydrogen bond between W3 and the water cluster in the ribose-34 pocket connects the new water cluster lined up by W1–W6. There is no electron density observable for the side chain of Gln107. Instead W5 occupies this position. c) Overlay of *lin*-benzoguanine **1** (C cyan, water molecules cyan; PDB code: 2Z7K[21]) and *lin*-benzohypoxanthine **8a** (C green, water molecules green; PDB code: 3S1G) in the active site of *Z. mobilis* TGT.

the side chains of Met260 and Tyr106 and, similar to the natural substrates guanine and preQ$_1$, their aminopyrimidinone ring engages in a complex hydrogen-bonding pattern with the protein that involves the side chains of Asp102, Asp156, Gln203, and the backbone NH of Gly230 (Figure 2a; compound **1**).[12,13] The *lin*-benzohypoxanthines lack the exocyclic NH$_2$ group at C(6) and, therefore, were expected to lose hydrogen bonds to the side chains of Asp102 and Asp156, respectively.

Synthesis: The synthetic route towards the different new inhibitors (Schemes 1–3) follows a previously reported strategy, starting from benzimidazole-5-carboxylic acid (**2**).[12,13] Esterification, nitration, and N-protection yielded two isomers that were separated chromatographically on a 40 g scale. Each isomer was brominated at C(2) to furnish the building blocks **3** and **4**, respectively, which were both used in the course of the syntheses (Scheme 1). Substitution of isomer **4** at C(2) with different primary amines gave 2-aminobenzimidazoles **5a–d**, which were reduced to the 2,6-diamino derivatives **6a–d**. Cyclization with either formamide or formamidinium acetate led to the formation of the pyrimidinone ring in **7a–d**, which were deprotected to yield *lin*-benzohypoxanthines **8a–d** directing substituents at C(2) into the ribose-33 pocket.

The *lin*-benzohypoxanthines that bear substituents to fill the ribose-34 pocket were prepared in a similar fashion, starting from isomer **3**. Because the imidazole protecting group is on the opposite side in this isomer, derivatization at C(4) is sterically less demanding and therefore facilitated. Following a literature procedure, benzimidazoles **9a**,**b** were prepared in eight steps from **3** (Scheme 2).[13] The presence

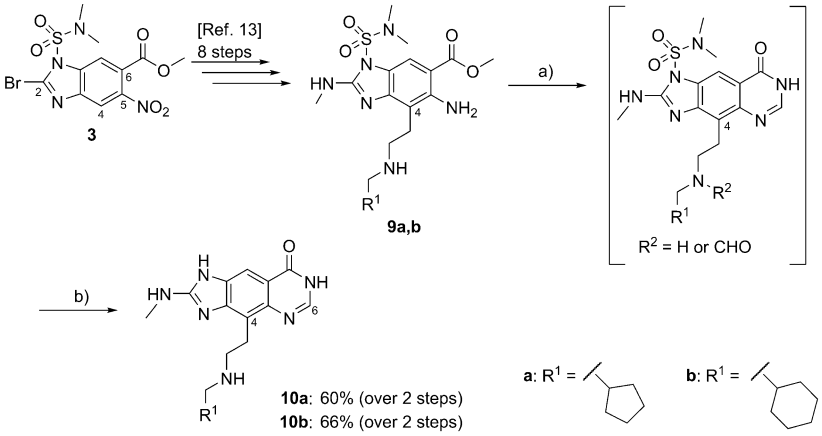

Scheme 2. Synthesis of *lin*-benzohypoxanthines **10a**,**b**: a) formamide, 140 °C, 18–22 h; b) HCl, MeOH, 65 °C, 18–24 h; 60–87 % (over two steps).

of the substituents at C(4) in **9a**,**b** mandated harsher conditions for the following cyclization step relative to the transformation of C(2)-substituted **6a–d** (Scheme 1). Stirring **9a**,**b** at 140 °C for several hours in formamide as solvent provided a mixture of the desired protected *lin*-benzohypoxanthines together with a side product in which the ethylamino group at C(4) was additionally N-formylated. Gratifyingly, both the N,N-dimethylsulfamoyl protecting group and the undesired N-formyl group were removed with HCl to furnish target compounds **10a**,**b**.

For the synthesis of the C(6)−N-monoalkylated *lin*-benzoguanines **11a**,**b**, the ring closure of an appropriate isatoic anhydride derivative with S-methylisothioureas **12a**,**b**, respectively, was envisaged.[19] Whereas **12a** was commercially available, the required ethyl derivative **12b** was prepared starting from N,N′-bis-Boc-protected (Boc = *t*-butyloxycarbonyl) S-methylisothiourea **13**, which was treated with EtI to afford N-ethylisothiourea **14** (Scheme 3).[20] Deprotection with trifluoroacetic acid gave the desired compound **12b**. For

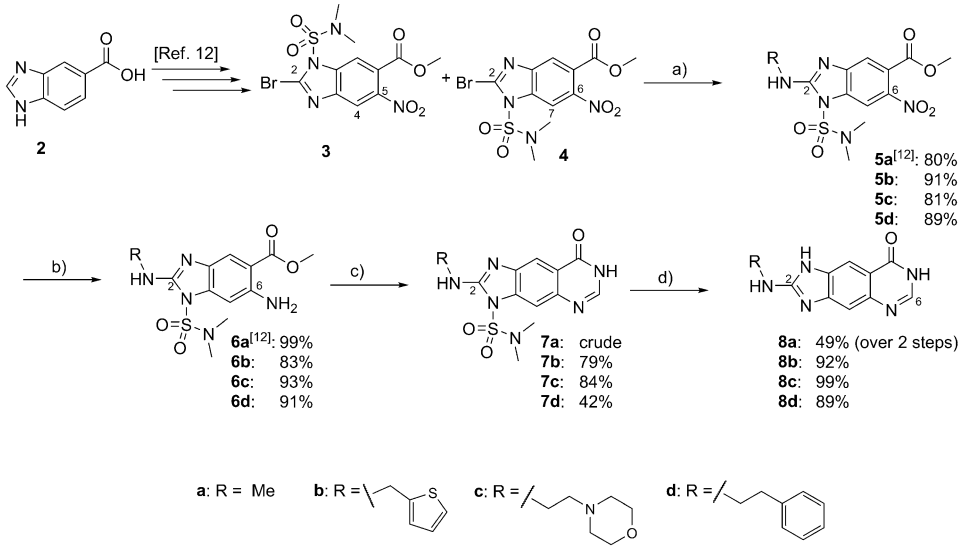

Scheme 1. Synthesis of *lin*-benzohypoxanthines **8a–d**: a) RNH$_2$, EtOAc, or EtOH, 0–25 °C, 1–7 h; 80–91 %; b) Zn, AcOH/H$_2$O, 25 °C, 20–60 min; 83–99 %; c) formamide, 140 °C, 18 h, crude; or formamidinium acetate, EtOH, 80 °C, 20–22 h; 42–84 %; d) HCl, MeOH, 65 °C, 30 min; 49–99 %.

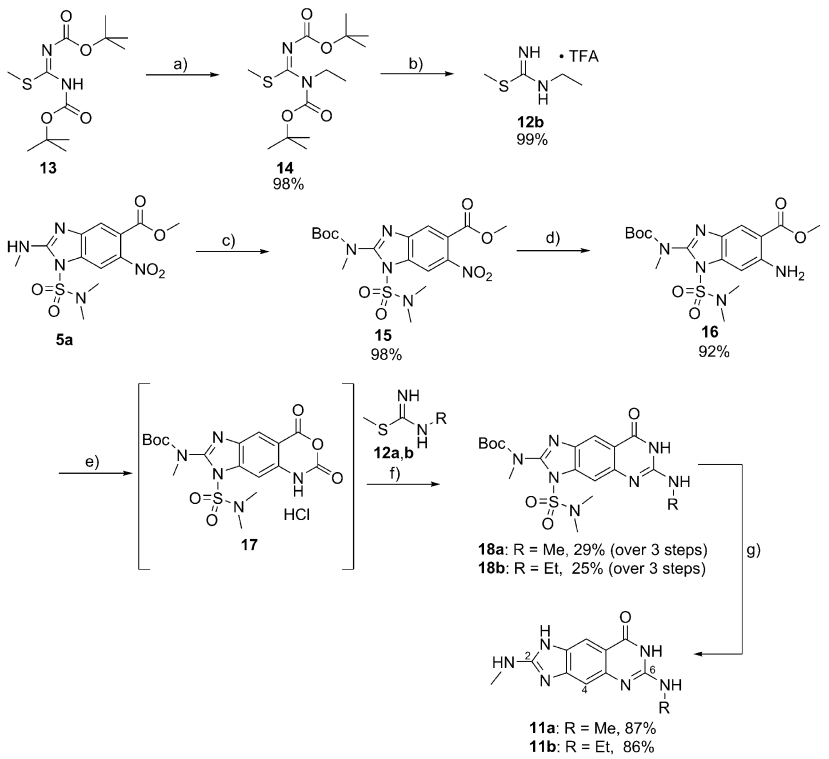

Scheme 3. Synthesis of the alkylated *lin*-benzohypoxanthines **11a**,**b**: a) K_2CO_3, EtI, acetone, 56 °C, 18 h; 98 %; b) TFA, CH_2Cl_2, 25 °C, 45 min; 99 %; c) Boc_2O, DMAP, Et_3N, THF, 25 °C, 17 h; 98 %; d) Zn, AcOH/H_2O, 25 °C, 60 min; 92 %; e) LiOH, MeOH/H_2O, 80 °C, 2 h; then triphosgene, THF, 0 to 25 °C, 2.5 h; f) **12a** or **12b**, Na_2CO_3, Me_2SO, 80 °C, 2 h; **18a**: 29 % (over 3 steps), **18b**: 25 % (over three steps); g) HCl, MeOH, 65 °C, 30 min; **11a**: 87 %, **11b**: 86 %. Boc_2O = dicarbonic acid di-*tert*-butyl ester, DMAP = 4-(dimethylamino)pyridine, DMF = N,N-dimethylformamide, TFA = trifluoroacetic acid, THF = tetrahydrofuran.

the cyclization, it was advantageous to protect the amino group at C(2). The Boc-protected benzimidazole **15** was obtained from **5a** and subsequently reduced to give **16**. Saponification yielded the anthranilic acid, which was treated with triphosgene to furnish isatoic anhydride **17** that was directly used in the following step. Contrary to the results of Coppola et al.,[19] the cyclization reaction in the absence of Boc protection gave an inseparable mixture of isomers. However, when isatoic anhydride **17** was used, the desired *lin*-benzoguanines **18a** and **18b** with alkylated exocyclic NH_2 groups at C(6) could be isolated in pure form. Final deprotection gave the target molecules **11a** and **11b**.

Biological activity: Competitive inhibition constants K_i were obtained at pH 7.3 in 100 mM HEPES buffer at 37 °C by a radioactive assay using [8-^{3}H]guanine, as described in the literature.[6,12,21] The *lin*-benzoguanine derivatives with an exocyclic NH_2 group show by far the strongest inhibition (Table 1; compounds **19a–d** and **20a**,**b**) with K_i values in the range of 2–58 nM.[12,13] The removal of the exocyclic NH_2 group in the corresponding *lin*-benzohypoxanthines **8a–d** (with substituents for the ribose-33 pocket) and **10a**,**b** (with substituents for the ribose-34 pocket) drastically reduces the affinity by a factor of 80–680 and yields K_i values in the range near 1 μM. Unexpectedly, monoalkylation at the exocyclic NH_2 group of the *lin*-benzoguanines reduces the potency even further and K_i values are now in the double-digit micromolar range. N-Methylated **11a** shows a 480-fold lower binding affinity relative to the NH_2 derivative **19a**, and N-ethylated **11b** binds even more weakly by a 700-fold factor. The origins of these large differences in binding strength become apparent in the discussion of the cocrystal structures (see below).

Physicochemical properties: We calculated clog*D* and clog*P* values and conducted measurements to analyze how the removal of the exocyclic NH_2 group in *lin*-benzohypoxanthines or its monoalkylation in *lin*-benzoguanines affects the physicochemical properties of the ligands. Both changes lead to more positive clog*D* and clog*P* values (calculated using ACD/Labs software; compare the 2-methylamino compounds **8a** and **11a,b** to **19a**; Table 1),[22,23] although all compounds remain highly hydrophilic. Upon the introduction of substituents at C(2) or C(4), the differences that result from the changes at C(6) increasingly vanish and become masked by the effects from the added substituents.

Measurements of the parallel artificial membrane permeability (PAMPA) scores[24] were performed to estimate differences in membrane permeability between the three types of ligands. The majority of the highly polar compounds do not penetrate the membrane (Table 1), with only two rated as "medium" due to accumulation in the membrane. Differences between the three ligand classes were not observed, as the highly polar 2-aminoimidazole moiety presumably dominates the behavior of all systems.

Classical potentiometric titrations to determine the pK_a values of the ligands were not feasible due to the low solubility of the *lin*-benzopurines. Instead, measurements were conducted by parallel capillary electrophoresis.[25] The pK_a values for *lin*-benzoguanines **19a**,**b** had been previously determined by photometric titration,[12] and the new data were found to be in good agreement (Table 1SI in the Supporting Information). The pK_a values for the 2-aminoimidazolium moiety (5.1–5.7) and N(7)H (>10) are similar for all three ligand classes. In contrast, the removal of the exocyclic NH_2 group at C(6) strongly increases the acidity of N(5)H$^+$ and lowers the pK_a from values around 4.0–4.4 in the *lin*-benzo-

Table 1. Inhibition constants K_i, c log D (calculated logarithmic distribution constant for *n*-octanol/water at pH 7.4) and c log P (calculated logarithmic partition constant for *n*-octanol/water) values, PAMPA scores, and pK_a values for *lin*-benzohypoxanthines and *lin*-benzoguanines.

		X	K_i [nM]	c log D[a] (pH 7.4)	c log P[a]	PAMPA score Pe [10^{-6} cm s^{-1}]	category	pK_a measurements N(7)H	N(3)H$^+$	N(5)H$^+$
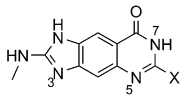	**19a**	NH_2	58 ± 36[12]	−0.33	−0.05	0.00[b]	medium	>10	5.7	4.4
	8a	H	6500 ± 2900	0.18	−0.19	0.00	low	>10	5.6	1.8
	11a	NHMe	28050 ± 11970	0.18	0.47	0.00	low	n.d.[c]	5.6	4.2
	11b	NHEt	40830 ± 4270	0.72	0.97	0.05	low			
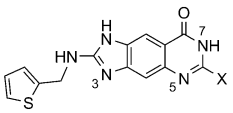	**19b**	NH_2	35 ± 9[2]	1.09	1.41	0.00[b]	medium	>10	5.5	4.0
	8b	H	2900	1.76	1.27	0.03	low	>10	5.1	2.0
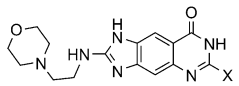	**19c**	NH_2	6 ± 6[12]	−0.89	−0.45	0.00	low			
	8c	H	4100	−0.22	−0.59	0.05	low			
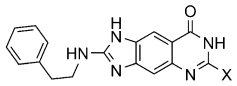	**19d**	NH_2	10 ± 3[12]	1.76	2.04					
	8d	H	3700	2.37	1.90					
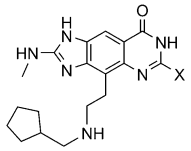	**20a**	NH_2	2 ± 1[13]	−0.87	1.78	0.00	low			
	10a	H	740 ± 170	−0.57	1.65	0.04	low			
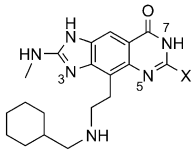	**20b**	NH_2	4 ± 2[13]	−0.23	2.31	0.09	low			
	10b	H	1100 ± 370	−0.10	2.17	0.00	low	n.d.[c]	5.3	n.d.[c]

[a] Calculated using ACD/Labs.[23] [b] Accumulation in membrane, hence the compound is categorized as medium. [c] n.d. = could not be determined with the applied method.

guanines to 2.0 and below in the *lin*-benzohypoxanthines (Table 1). This may have a large impact on the binding mode as it is assumed that N(5) is protonated in the active site to undergo hydrogen bonding to the presumably deprotonated side chain of Asp102.[21,26] The *lin*-benzohypoxanthines have to pay a greater energetic penalty for protonation at N(5) relative to the *lin*-benzoguanines. The data indicate that the parent tricyclic scaffolds are predominantly in their unprotonated form under assay conditions (pH 7.3), although Poisson–Boltzmann calculations for *lin*-benzoguanines suggest an increase of the pK_a value of the 2-aminoimidazolium moiety upon binding in the enzyme pocket.[21]

X-ray cocrystal structures of *lin*-benzohypoxanthines: For the four ligands **8a–c** and **10a**, crystal structures in complex with TGT could be obtained with a maximum resolution between 1.53 and 1.82 Å (Table 2). The tricyclic aromatic ring system of 2-amino-*lin*-benzohypoxanthines (Figure 2b) binds in a way that is similar to the closely related 2-amino-*lin*-benzoguanines (Figure 2a) in the guanine subpocket. In all structures, the tricyclic scaffold is fixed by means of hydrogen bonds to the side chains of Asp156 and Gln203, the backbone NH of Gly230, and the backbone C=O groups of Leu231 and Ala232. The interaction with the backbone C=O of Leu231 can be assumed to be rather strong due to the charge assistance provoked by the most likely protonation of the 2-aminoimidazole core of the ligand and the additional Glu235, which polarizes the addressed backbone carbonyl even further.[12] The tricyclic aromatic skeleton is sandwiched between Tyr106 and Met260, thus undergoing favorable π-stacking interactions. As reported for the cocrystal structures with *lin*-benzoguanines, the binding of *lin*-benzohypoxanthines induces a *cis*-peptide bond conformation between Val262 and Gly263 (not shown).[21]

For the unsubstituted ligand **8a**, a dataset with a resolution of 1.82 Å showed a well-defined electron density for the ligand and the surrounding water molecules within the active site (Figure 2b; for hydrogen-bonding lengths, see Figure 1SI in the Supporting Information). The comparison of this structure with that previously published for *lin*-benzoguanine **1** (PDB code: 2Z7K[21]) revealed that removal of the exocyclic amino functionality at C(6) leads to a rotation of the side chain of Asp102 within the guanine subpocket, away from the bound ligand (Figure 2c). Instead, it now undergoes hydrogen bonding to the side chain NH_2 of Asn70 and the backbone NH of Thr71. This interaction is already known from apo structures of TGT (Figure 2SI in the Supporting Information)[27] and from cocrystal structures with ligands bound to the guanine subpocket that lack a hydrogen-bond donor in a fitting distance to the carboxyl functionality of Asp102 (e.g., PDB code: 1F3E;[4] Figure 3SI in the Supporting Information). The emerging space at the bottom of

Table 2. X-ray cocrystal structures: data collection and refinement statistics.

	8a	**8b**	**8c**	**10a**	**11a**	**11b**
PDB code	3S1G	3GEV	3V0Y	3SM0	3RR4	3TLL
no. crystal used	1	1	1	1	1	1
λ [Å]	0.91841	0.91841	0.91841	0.91841	0.91841	0.91481
space group	*C*2	*C*2	*C*2	*C*2	*C*2	*C*2
a [Å]	90.8	91.2	91.0	91.0	90.7	91.2
b [Å]	64.8	64.7	64.9	64.9	64.8	64.8
c [Å]	70.6	70.3	70.6	71.2	70.5	70.3
β [°]	95.9	95.9	95.9	96.4	96.0	96.0
resolution range [Å]	30–1.82	30–1.53	30–1.65	25–1.57	30–1.68	30–1.37
unique reflections	35920 (1807)[a]	54813 (2380)[a]	45274 (2008)[a]	54458 (2425)[a]	45107 (2115)[a]	81623 (3991)[a]
$R(I)_{sym}$ [%][b]	5.8 (24.1)[a]	6.3 (43.8)[a]	4.7 (29.9)[a]	5.6 (27.0)[a]	5.9 (28.7)[a]	3.1 (13.1)[a]
completeness [%]	97.9 (98.2)[a]	89.3 (77.1)[a]	95.9 (81.8)[a]	93.8 (83.9)[a]	96.3 (90.9)[a]	95 (94.5)[a]
redundancy	2.7 (2.2)[a]	2.6 (1.6)[a]	2.5 (2.2)[a]	2.7 (2.2)[a]	2.9 (2.3)[a]	2.7 (2.7)[a]
I/σ (I)	17.9 (3.6)[a]	16.0 (1.9)[a]	19.0 (2.6)[a]	16.2 (2.7)[a]	19.5 (2.1)[a]	25.2 (8.1)[a]
resolution range [Å]	30–1.82	10–1.53	30–1.65	25-1.57	30–1.68	30–1.37
reflections used in refinement	34666	51600	43009	51761	42831	76018
final *R* values						
R_{free} (F_o; $F_o > 4\sigma F_o$)[c]	21.4 (20.0)	20.9 (19.1)	21.8 (20.5)	20.3 (18.8)	20.0 (19.0)	16.8 (16.3)
R_{work} (F_o; $F_o > 4\sigma F_o$)[d]	16.3 (15.3)	17.4 (16.0)	17.4 (16.4)	16.4 (15.4)	15.9 (15.0)	12.6 (12.4)
no. of atoms (non-hydrogen)						
protein atoms	2794	2723	2734	2763	2864	2873
water molecules	249	207	246	291	290	367
ligand atoms	16	16	16	25	18	19
RMSD, angle [°]	1.9	2.3	2.0	2.2	2.0	2.1
RMSD, bond [Å]	0.007	0.010	0.008	0.009	0.008	0.013
Ramachandran plot[e]						
most favored regions [%]	95.0	96.3	95.7	94.5	94.9	96.2
additionally allowed regions [%]	4.6	3.4	4.0	4.9	4.8	3.5
generously allowed regions [%]	0.4	0.3	0.3	0.6	0.3	0.3
mean *B* factors [Å^2]						
protein atoms	15.1	13.7	19.4	17.6	15.8	14.0
water molecules	24.5	22.3	28.7	28.6	25.7	28.3
ligand atoms	12.7	15.6	23.8	15.0	14.8	12.4

[a] Values in parentheses are statistics for the highest resolution shell. [b] $R(I)_{sym} = [\Sigma_h \Sigma_i |I_i(h) - \langle I(h)\rangle| / \Sigma_h \Sigma_i I_i(h)] \times 100$, in which $\langle I(h)\rangle$ is the mean of the $I(h)$ observation of reflection h. [c] $R_{work} = \Sigma_{hkl} |F_o - F_c| / \Sigma_{hkl} |F_o|$. [d] R_{free} was calculated as shown for R_{work} but on refinement-excluded 5% of data. [e] Calculated with Procheck.[38]

the guanine subpocket provoked by the Asp102 rotation is filled with water molecules, which form a well-defined six-membered network (W1–W6) (Figure 2b; for residue identifiers, see Table 2SI in the Supporting Information; for hydrogen-bonding lengths, see Figure 1SI in the Supporting Information).[28] W1 solvates Asp156, whereas W3 interacts through a hydrogen bond with N(5) of the ligand. A contact to the rotated Asp102 is built by means of W5 and W6. Water W3 is also connected to the five-membered water cluster, which is well conserved between Asp102 and Asp280 and has already attracted attention in preceding studies[14] (Figure 2a and c). For the side chain of Gln107 (not shown), which flanks the guanine subpocket, no electron density is visible at the applied contour level. It seems to be solvent-exposed without directed interactions.

For the complexes of ligands **8b** and **8c**, datasets with resolutions of 1.53 and 1.65 Å, respectively, were obtained (Figure 3; for hydrogen-bonding lengths see Figures 4SI and 5SI in the Supporting Information). Their binding mode is analogous to the one observed for **8a**. Asp102 is rotated away from the bound ligand, and the newly formed space is filled with five well-defined water molecules that are equally positioned to W1–W4 and W6 in the complex of **8a** (Figure 3b). The water network described above is apparently highly conserved in the crystal structures. The position of W5 is different due to a change in the network pattern. Gln107 adopts a position facing the guanine subpocket in the structures with **8b**,**c** and establishes a directed hydrogen bond to W6 (Figure 6SI in the Supporting Information). In the complex with **8c**, the side chain C=O of Gln107 almost adopts the position of W5. A similar situation is found in the cocrystal structure with **8b**, but Gln107 is slightly tilted relative to **8c**, and the side chain O-position shifted by about 0.4 Å. Nevertheless, the Gln107 side chain interacts with W6 directly in **8c** as well. In the two complexes **8b** and **8c**, W3 again interacts with N(5) of the ligand. The water positions W1, W2, W4, and W6 also occur in the apo structure (PDB code: 1P0D;[4] Figure 2SI in the Supporting Information). In the unoccupied active site, Gln107 shows a different conformation from **8b**,**c** (Figure 6SI in the Supporting Information). Nevertheless, in this conformation we also observed a hydrogen bond from the terminal carboxamide C=O to W6 (2.5 Å). Similar to the reported cocrystal structures of C(2)-substituted *lin*-benzoguanines, there is no reasonable electron density seen for the C(2) side chains in **8b** and **8c**; hence they can be assumed to be highly flexible or

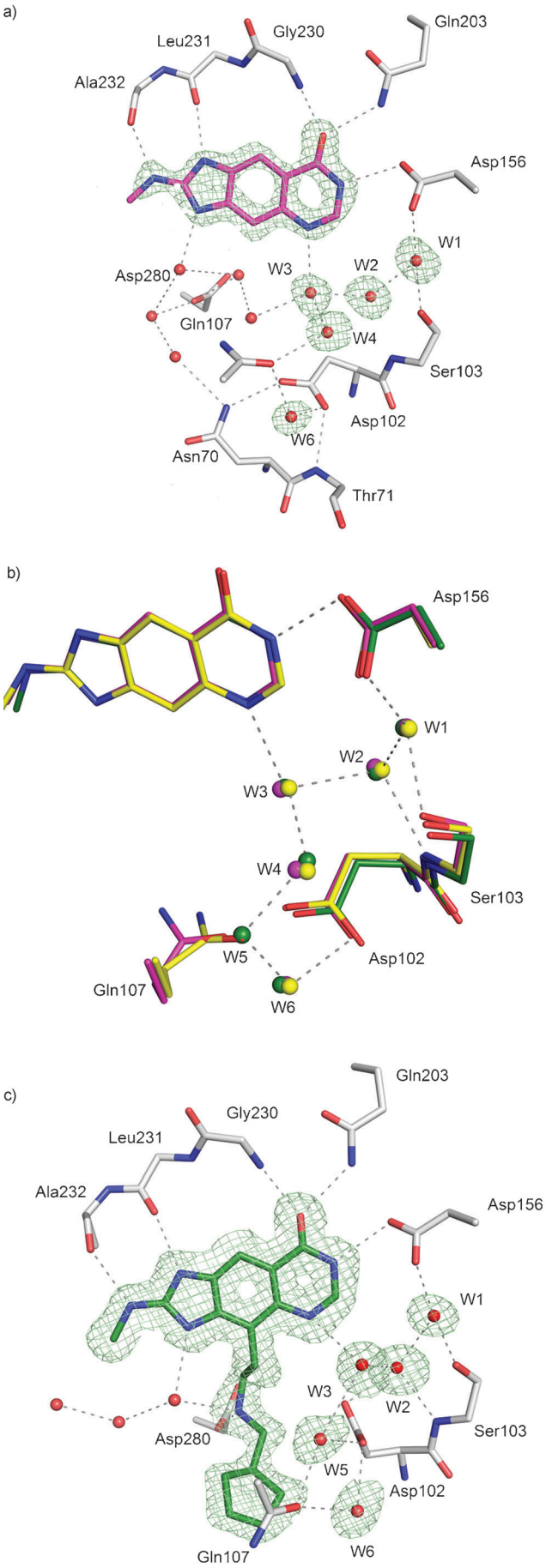

scattered over multiple conformations.[21] These side chains are most likely directed towards the flat and solvent-exposed ribose-33 pocket. As a driving force behind the rotation of Gln107 in the complexes of **8b** and **8c**, an influence of the flexible C(2) side chain on the active site solvation pattern is imaginable.

A different orientation of Asp102 and, in consequence, a varied water network can be found in the complex of TGT with **10a** (Figure 3c). The parent scaffold contains an extended substituent on C(4) of the tricycle that points into the ribose-34 pocket. In analogy to preceding studies, the ethylamine linker is used to occupy the polar ribose-34 pocket, thereby displacing the water cluster around the most likely negatively charged Asp102 and Asp280.[13,14] The terminal cyclopentyl ring undergoes a hydrophobic interaction with Val45 and Leu68 that form the apolar bottom of the ribose-34 pocket. In contrast to the complexes with **8a–c**, the side chain of Asp102 cannot be solvated by an interaction to Asn70 and Thr71. The C(4) substituent of the ligand hinders the complete rotation of Asp102, hence it stays in a tilted intermediate position. However, this small rotation also opens space in the guanine subpocket, which is filled with water molecules that build a network (W1–W3, W5, and W6). W1, W2, W5, and W6 are at the conserved positions as can be seen in the structures with **8a–c**. Because of the tilted position of Asp102, the former water molecule W4 is displaced and W3 now occupies a shifted position and undergoes hydrogen-bonding interactions with Asp102, W2, W5, and N(5) of the ligand (for hydrogen-bonding lengths, see Figure 7SI in the Supporting Information).

X-ray cocrystal structures of C(6)−N-alkylated *lin*-benzoguanines: For the complexes with C(6)−N-alkylated *lin*-benzoguanines **11a** and **11b**, datasets with resolutions of 1.68 and 1.37 Å, respectively, were obtained (Figure 4). The adaptation of the guanine subpocket to the binding of C(6)−N-alkylated *lin*-benzoguanines matches very well with the described binding of *lin*-benzohypoxanthines. Due to the spatial requirements of the C(6)−N-alkyl moieties, the hy-

Figure 3. X-ray cocrystal structures of *lin*-benzohypoxanthines **8a–c** and **10a** bound to the active site of *Z. mobilis* TGT. a) Cocrystal structure of **8b** (C_{ligand} magenta) bound to the active site of TGT (PDB code: 3GEV). There is no reasonable electron density observable for the N-ethylthiophene side chain, which was already found to be highly disordered in an earlier cocrystal structure of **19b** bound to TGT.[21] Gln107 forms with its side chain C=O a bridging hydrogen bond between W4 and W6 ($d(O_{Gln107}\cdots O_{W4}) = 2.9$ Å and $d(O_{Gln107}\cdots O_{W6}) = 2.7$ Å). After detailed visual inspection of the electron density maps and the *B* values, the nitrogen/oxygen orientation of the Gln107 carboxamide side chain has been rotated by 180° and deviates from the coordinate file deposited in the PDB. b) Superposition of **8a** (C_{ligand} green), **8b** (C_{ligand} magenta), and **8c** (C_{ligand} yellow) in complex with TGT. Illustrated are the ligand, the discussed water molecules (shown in **8a**: green, **8b**: magenta, and **8c**: yellow), and the residues involved in the water network. Water positions W1–W4 and W6 are highly conserved in the three structures. The bridging position of W5 in the complex of **8a** is adopted by the side chain C=O of Gln107 in the complexes of **8b**,**c** (Figure 6SI in the Supporting Information). c) Cocrystal structure of **10a** bound to the active site of TGT (PDB code: 3SM0).

drogen bonds to Asp102 are also not formed in these complexes. Hence, Asp102 also rotates out of the ligand binding pocket here and interacts with Asn70 and Thr71. Water molecules fill the cavity beneath the ligand but form a different pattern than the complexes with **8a–c** and **10a** (see the Supporting Information). In the cocrystal structure with **11a**, three water molecules (W1–W3) take the above-mentioned enabled space (Figure 4a). W1 is located at a supposedly energetically less favorable position surrounded by the hydrophobic parts of the side chains of Asp102, Ile201, and Met153 (Figure 8SI in the Supporting Information) and only forms hydrogen bonds to the protein with the side chain OH and the backbone NH of Ser103. W1 also interacts with W2, which forms hydrogen bonds to Tyr258 (not shown) and W3. Hydrogen bonds are established between W3 and N(5) of the ligand and one of the well-conserved water molecules between Asp102 and Asp280. Extending through three following water molecules (W4–W6), this network also finds its endpoint in an interaction with the side chain of Asp102. The C(6)–N-alkyl moieties of **11a** and **11b** both adopt the s-*cis* conformation in the cocrystal structures. An s-*trans* orientation is sterically hindered as it would create a consequent clash if the side chain of Asp156 will not move out of space as Asp102 does in all the studied complexes. Likely, the movement of Asp102 is also more favored as this movement is expected to occur during catalysis.[18] Furthermore, the s-*cis* conformation is also the preferred one in solution, as revealed by DFT calculations at the B3LYP/6-311G(d,p) level of theory (Figure 9SI in the Supporting Information). When comparing the cocrystal structures of **11a** and **11b**, well-conserved positions for the water molecules W2–W6 can be observed. W1 is displaced by the additional carbon of the N-ethyl residue of **11b**, which in one of the two observable orientations (occupancy 36%) points into the hydrophobic area of the guanine subpocket around Ile201, Met153, and Ser103 (Figure 4b; see also Figure 10SI in the Supporting Information). This leaves both the NH and OH groups of Ser103 unsolvated. The orientation of the terminal carbon of the N-ethyl moiety additionally produces steric clashes with the side chain of Met260 that can in consequence only be partly observed in the highly conserved conformation (Figure 10SI in the Supporting Information). In the second orientation (64% occupancy), the terminal carbon of the N-ethyl group of **11b** occurs in a nearly 180° rotated orientation and is unfavorably directed towards the backbone NH of Tyr106. Only when the terminal carbon of the N-ethyl moiety adopts the latter conformation does the side chain of Met260 assume its highly conserved position with a corresponding occupancy.

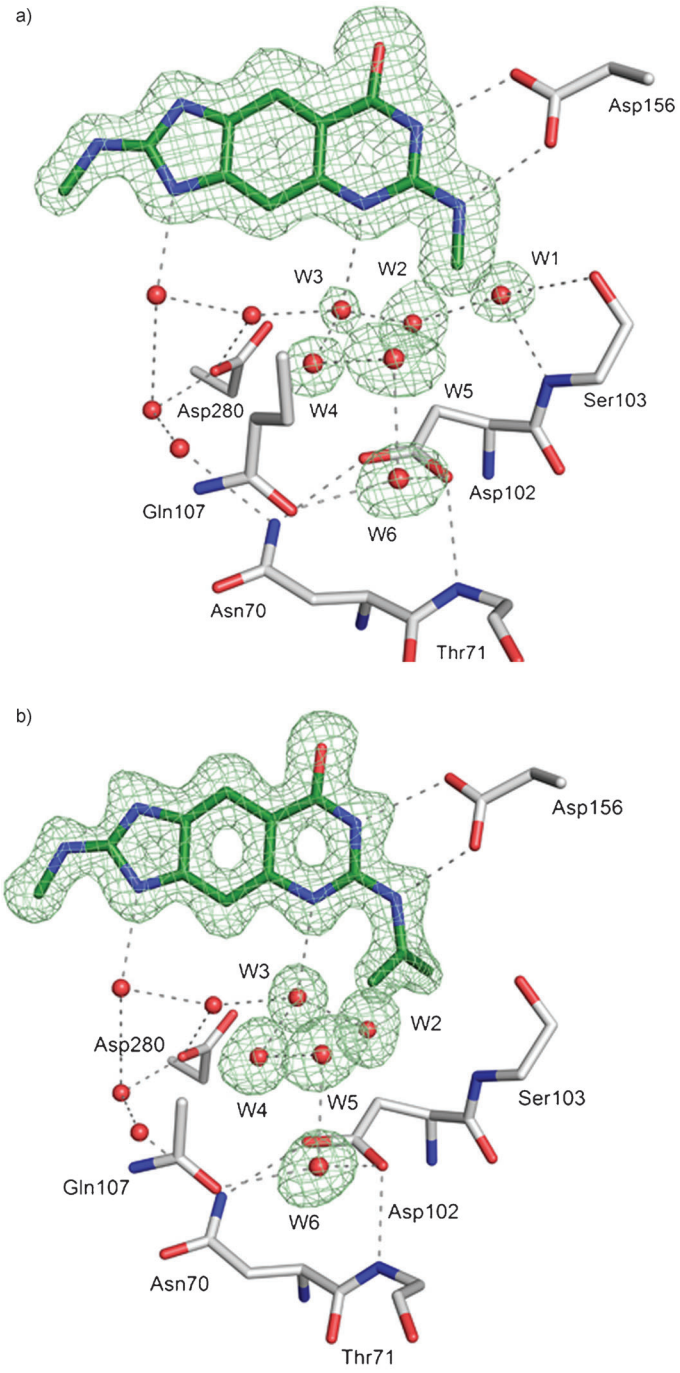

Figure 4. X-ray cocrystal structures of *Z. mobilis* TGT with C(6)–N-monoalkylated *lin*-benzoguanines **11a**,**b**. a) Cocrystal structure of **11a** bound to the active site of TGT (PDB code: 3RR4). For clarity, the residues Met153 and Ile201 that surround W1 are not shown (Figure 8SI in the Supporting Information). Tyr258, hidden behind the ligand, is also not displayed. b) Cocrystal structure of **11b** bound to the active site of TGT (PDB code: 3TLL). Two conformations of the N-ethyl moiety are observed, one with an occupancy of 36%, with the terminal methyl group pointing towards the hydrophobic cavity around Ser103, and a second, with an occupancy of 64%, in which the terminal methyl group is nearly flipped by 180°, thus facing the tricyclic ligand scaffold.

Origin of the differences in biological activity between *lin*-benzoguanines, their N-monoalkylated derivatives, and *lin*-benzohypoxanthines: Taken together, the results from the biological and physicochemical assays and from biostructure analysis allow a detailed insight into the molecular recognition of *lin*-benzoguanines and *lin*-benzohypoxanthines at the active site of TGT. The *lin*-benzohypoxanthines are 80–680 times less potent than the corresponding *lin*-benzoguanines (Table 1). The pK_a measurements (Table 1) suggest that

N(5) (pK_a values 1.8–2.0) of the *lin*-benzohypoxanthines most probably is not protonated in this part of the scaffold, in contrast to the *lin*-benzoguanines, with corresponding pK_a values 4.0–4.4. Therefore, interaction of the ligand with the carboxylate side chain of Asp102 is unfavorable, which causes this side chain to rotate away from the ligand into a conformation similar to the one adopted in the apoenzyme. However, the largest part of the loss in binding energy, when changing to the *lin*-benzohypoxanthine ligands, most probably originates from the loss of the two short ionic hydrogen bonds, which the exocyclic C(6)–NH_2 groups of the *lin*-benzoguanines form with the carboxylates of Asp102 (e.g., in the complex of **1**: d(N···O) = 2.8 Å) and Asp156 (d-(N···O) = 2.8 Å). Also, a weaker interaction with the OH of Ser103 (d(N···O) = 3.7 Å) is lost. The import of a well-conserved water cluster, which consists of 5 to 6 molecules that form a network among each other and a series of hydrogen bonds to the protein, does not compensate for the loss of the hydrogen bonds from the C(6)–NH_2 to the anionic side chains of Asp102 and Asp156.

The bulk of the C(6)–N-methyl and C(6)–N-ethyl groups in ligands **11a** and **11b** prevents an interaction of the ligand with the side chain of Asp102, which turns away to adopt the conformation seen in the apoenzyme and in the complexes of *lin*-benzohypoxanthines **8a–c**. Compared to *lin*-benzoguanines with unsubstituted C(6)–NH_2 group, the two hydrogen bonds to the carboxylate of Asp102 are lost, as well as the weaker interaction with the OH group of Ser103. In the complex of **11a**, a water cluster W1–W6 is imported into the space vacated by the conformational change of Asp102. However, this cluster is energetically less favorable than the cluster in the structures of *lin*-benzohypoxanthines **8a–c**, as some of the water molecules are forced by the C(6)–N-methyl group into less favorable, more hydrophobic environments. In particular, W1 loses the ionic hydrogen bond to the side chain of Asp156, which is seen in the complexes of **8a–c** (Figure 8SI in the Supporting Information), and the water network chain to N(5) through W2 and W3 is ruptured. As a result, C(6)–N-methylated **11a** (K_i = 28′050 nM) has a 480-fold lower binding affinity than the NH_2 derivative **19a**. The stability of the complex of N-ethylated **11b** (K_i = 40′830 nM) is even further reduced by a factor of 700-fold relative to **19a**. First of all, the desolvation of the ethyl derivative requires more energy, particularly as the ethyl group does not find a favorable hydrophobic environment in the protein. Second, the ethyl substituent displaces W1 from the water cluster. Displacement of water molecules from an environment of uncharged residues appears to be related to a negligible effect in the free energy; however, large compensating contributions in enthalpy and entropy are observed.[29,30] If displacement from an environment with charged residues is attempted, an unfavorable free energy contribution can also be observed.[31] The latter is also given for the complexes studied here, because W1 is involved in interactions to the charged residue Asp156. Nevertheless, favorable replacements of water molecules by N-alkyl moieties have also been reported, for example, for inhibitors of catechol-O-methyltransferase.[32] Furthermore, the backbone NH and the OH group of Ser103 become fully desolvated, which should also reduce the overall binding affinity.

Conclusion

Here we have compared the properties of three series of ligands for *Z. mobilis* TGT: *lin*-benzoguanines, their C(6)–N-alkylated derivatives, and *lin*-benzohypoxanthines. Their physical properties are dominated by the highly polar, basic 2-aminoimidazole moiety, which is the origin of low partitioning and distribution constants and poor membrane permeability. A large difference in the measured pK_a value for the N(5)H^+ moiety, which shifts from approximately 4 in the *lin*-benzoguanines to around 2 in the *lin*-benzohypoxanthines may have a strong influence on the binding affinity to the protein. Whereas *lin*-benzoguanines bind with K_i values in the single- to double-digit nanomolar range, as a result of ionic hydrogen bonding of the aminopyrimidinone ring to two Asp side chains, *lin*-benzohypoxanthines only show affinities in the single-digit micromolar range or slightly below. The C(6)–N-alkylated *lin*-benzoguanines are even weaker ligands with K_i values in the double-digit micromolar range. The origin of the different binding affinities was investigated by X-ray cocrystal structure analysis. The tricyclic scaffold of all three ligand classes adopts the same binding geometry in the guanine recognition pocket. For the *lin*-benzohypoxanthines that lack the C(6)–NH_2, an ionic hydrogen bond to the carboxylate of Asp156, which remains in a conserved orientation, is lost. Furthermore, the carboxylate of Asp102 no longer binds to the ligand and changes its conformation to adopt a position seen in the apoenzyme, which is supposedly important in the catalytic mechanism. This conformational change opens up a space that is filled by a conserved water cluster. Although the water cluster undergoes several favorable interactions with the protein, they are not sufficient to compensate for the loss of ligand–protein ionic hydrogen bonding, and the overall binding affinity is strongly reduced. The structural data show that the bound C(6)–N-alkyl *lin*-benzoguanines maintain the double ionic hydrogen bonding to the side chain of Asp156. However, for steric reasons, the bulky C(6)–N-alkyl moiety prevents the interaction with the side chain of Asp102, which again switches to the orientation seen in the apoenzyme. The opened space is again filled by a water cluster, which nevertheless interacts in a less favorable way with the protein and the ligand. In particular, the cocrystal structure of the N-ethyl derivative **11b** shows a fully desolvated Ser103 residue along with the loss of a water contact to the adjacent charged Asp156 residue, which presumably causes the poorest binding affinity in the entire series. Together with our previous work on the substitution of the water cluster between the two side chains of catalytic Asp102 and Asp280,[12,21] this investigation documents that much remains to be learned about the energetics of such water clusters in

protein–ligand complexes and of the substitution of individual water molecules in these clusters by ligand parts. It is clear from this work that such an enhancement in the knowledge will have to rely on accurate, high-resolution X-ray cocrystal structure analysis such as that reported in this contribution. Small changes in the ligand may not only lead to losses/gains in protein–ligand hydrogen bonds but might also profoundly affect the solvation and the formation of contiguously connected water networks that mediate interactions in such a complex, which makes it even more difficult to assign accurate energetic quantities to lost/formed hydrogen bonds.

Experimental Section

Materials and general methods: Compounds **3**, **4**, **5a**, **6a**,[12] and **9a**,**b**[13] were prepared as described in the literature. In the following, the experimental details for the syntheses of compounds **8a–d**, **10a**,**b**, and **11a**,**b** are described. All other synthetic details and experimental data, NMR spectra, description of the pK_a measurements and PAMPA score, and the biological assay can be found in the Supporting Information. Crystallographic pictures were prepared using PyMol.[33]

General procedure 1 (GP 1) for the cyclization to the *lin*-benzohypoxanthines with formamide: A solution of the benzimidazole in anhydrous formamide was heated at 140 °C for 18–22 h under Ar and evaporated by bulb-to-bulb distillation (1 mbar, 140 °C).

General procedure 2 (GP 2) for the cleavage of the protecting group(s): *Method a*: The protected *lin*-benzopurine (1.0 equiv) was heated in concentrated aqueous HCl solution/MeOH 1:2 (2.0–6.0 mL) at 65 °C for 18–24 h, neutralized (pH 6–7) with saturated aqueous $NaHCO_3$ solution, and evaporated. The residue was suspended in MeOH, filtered, purified by preparative HPLC (Phenomenex, 50×21.1 mm, Gemini 5 μm, C18, 110 A, AXIA; flow rate 15 mL min^{-1}, H_2O +0.1 vol% HCOOH/MeCN 100:0 for 10 min, 100:0 to 80:20 within 40 min), and lyophilized to yield the free amine. *Method b*: The protected *lin*-benzohypoxanthine (1.0 equiv) was heated in 2 M aqueous HCl/MeOH 1:1 at 65 °C for 30 min and then evaporated. The residue was dissolved in H_2O and neutralized by addition of saturated aqueous $NaHCO_3$ solution. The white precipitate was removed by filtration and washed with H_2O.

2-(Methylamino)-1,7-dihydro-8*H*-imidazo[4,5-*g*]quinazolin-8-one (8a): According to GP 1, starting from **6a** (50 mg, 0.153 mmol) in anhydrous formamide (2.0 mL). The resulting crude **7a** was directly used according to GP 2a to yield **8a** (16 mg, 49% over two steps) as a white solid. M.p. >245 °C (decomp); ^{1}H NMR (300 MHz, 1 M NaOD in D_2O): δ=2.83 (s, 3H; NMe), 7.18 (s, 1H; H–C(4)), 7.64 (s, 1H; H–C(6)), 8.00 ppm (s, 1H; H–C(9)); ^{13}C NMR (100 MHz, 1 M NaOD in D_2O): δ=29.23 (NMe), 103.90 (C(4 or 9)), 104.46 (C(4 or 9)), 113.74 (C(8a)), 144.23 (C(9a)), 146.39 (C(3a)), 152.39 (C(4a)), 153.10 (C(6)), 170.93 (C(2)), 173.34 ppm (C(8)); IR (ATR): $\tilde{\nu}$=3540–2500 (br m), 1678 (s), 1649 (s), 1625 (s), 1568 (m), 1463 (m), 1375 (m), 1349 (m), 1279 (m), 1224 (m), 1197 (m), 1155 (m), 1099 (m), 985 (m), 920 (m), 841 (m), 783 (m), 694 cm^{-1} (m); HR-MALDI-MS: *m*/*z*: calcd (%) for $C_{10}H_{10}N_5O^+$: 216.0880; found: 216.0878 (100) $[M+H]^+$.

2-[(Thien-2-ylmethyl)amino]-1,7-dihydro-8*H*-imidazo[4,5-*g*]quinazolin-8-one (8b): According to GP 2a, starting from **7b** (53 mg, 0.13 mmol) to yield **8b** (36 mg, 92%) as a white solid. M.p. >198 °C (decomp); ^{1}H NMR (300 MHz, D_2O/TFA 95:5): δ=4.39 (s, 2H; CH_2), 6.52 (dd, *J*=5.1, 3.6 Hz, 1H; H–C(4′)), 6.66 (dd, *J*=3.6, 1.2 Hz, 1H; H–C(3′)), 6.89 (dd, *J*=5.1, 1.2 Hz, 1H; H–C(5′)), 7.20 (s, 1H; H–C(4)), 7.68 (s, 1H; H–C(6)), 8.65 ppm (s, 1H; H–C(9)); ^{13}C NMR (100 MHz, D_2O/TFA 95:5): δ=41.13 (CH_2), 101.37 (C(9)), 108.83 (C(4)), 116.09 (C(8a)), 125.97 (C(5′)), 126.67 (C(3′ or 4′)), 126.80 (C(3′ or 4′)), 130.86 (C(4a)), 133.26 (C(2′)), 135.96 (C(6)), 136.54 (C(9a)), 147.00 (C(3a)), 151.65 (C(2)), 158.96 ppm (C(8)); IR (ATR): $\tilde{\nu}$ = 3024 (br w), 1620 (s), 1594 (s), 1566 (s), 1454 (s), 1367 (w), 1289 (m), 1218 (w), 1093 (w), 913 (w), 851 (w), 786 (w), 695 cm^{-1} (m); HR-MALDI-MS: *m*/*z*: calcd (%) for $C_{14}H_{12}N_5OS^+$: 298.0757; found: 299.0787 (19), 298.0755 (100) $[M+H]^+$.

2-{[2-(4-Morpholinyl)ethyl]amino}-1,7-dihydro-8*H*-imidazo[4,5-*g*]quinazolin-8-one (8c): According to GP 2b, starting from **7c** (28 mg, 0.07 mmol). Flash chromatography (MCI gel; H_2O/MeCN 100:0 to 80:20), followed by lyophilization, yielded **8c** (20 mg, 99%) as a white powder. M.p. >160 °C (decomp); ^{1}H NMR (300 MHz, CD_3OD): δ=2.56 (t, *J*=4.5 Hz, 4H; $N(CH_2)_2$), 2.67 (br t, *J*≈6.3 Hz, 2H; CH_2CH_2NH), 3.57 (t, *J*=6.3 Hz, 2H; CH_2NH), 3.71 (br t, *J*=4.5 Hz, 4H; $O(CH_2)_2$), 7.44 (s, 1H; H–C(4)), 7.95 (s, 1H; H–C(6)), 7.96 ppm (s, 1H; H–C(9)); ^{13}C NMR (100 MHz, D_2O+1 drop TFA): δ=37.49 (CH_2NH), 52.24 (2C; $N(CH_2)_2$), 54.84 (CH_2CH_2NH), 63.65 (2C; $O(CH_2)_2$), 102.79 (C(9)), 109.49 (C(4)), 117.03 (C(8a)), 131.13 (C(4a)), 135.09 (C(3a)), 136.32 (C(9a)), 147.46 (C(6)), 152.68 (C(2)), 160.24 ppm (C(8)); IR (ATR): $\tilde{\nu}$= 3238 (br w), 1626 (s), 1610 (s), 1570 (m), 1462 (s), 1381 (w), 1297 (s), 1205 (w), 1111 (s), 1003 (m), 911 (w), 866 (m), 786 cm^{-1} (m); HR-MALDI-MS: *m*/*z*: calcd (%) for $C_{15}H_{19}N_6O_2^+$: 315.1564; found: 316.1598 (15), 315.1562 (100) $[M+H]^+$.

2-[(2-Phenylethyl)amino]-1,7-dihydro-8*H*-imidazo[4,5-*g*]quinazolin-8-one (8d): According to GP 2b, starting from **7d** (32 mg, 0.077 mmol). Flash chromatography (MCI gel; H_2O/MeCN 100:0 to 80:20), followed by lyophilization, yielded **8d** (26 mg, 89%) as a white solid. M.p. >250 °C; ^{1}H NMR (300 MHz, CD_3OD): δ=3.06 (t, *J*=7.2 Hz, 2H; CH_2CH_2NH), 3.77 (t, *J*=7.2 Hz, 2H; CH_2NH), 7.17–7.23 (m, 1H; H–C(4′)), 7.28–7.34 (m, 4H; H–C(2′,3′,5′,6′)), 7.65 (s, 1H; H–C(4)), 8.13 (s, 1H; H–C(6)), 8.92 ppm (s, 1H; H–C(9)); ^{13}C NMR (100 MHz, $(CD_3)_2SO$): δ=34.44 (CH_2CH_2NH), 44.26 (CH_2NH), 106.37 (C(9)), 107.02 (C(4)), 117.76 (C(8a)), 126.47 (C(4′)), 128.36 (2 C; C(2′,6′)), 128.92 (2 C; C(3′,5′)), 130.07 (C(4a)), 135.78 (C(1′)), 138.12 (2 C; C(6,9a)), 144.98 (C(3a)), 151.94 (C(2)), 160.14 ppm (C(8)); IR (ATR): $\tilde{\nu}$=3213 (w), 2988 (w), 2901 (w), 1705 (s), 1668 (s), 1657 (s), 1486 (m), 1319 (m), 1298 (m), 1047 (w), 902 (w), 873 (m), 752 cm^{-1} (m); HR-MALDI-MS: *m*/*z*: calcd (%) for $C_{17}H_{16}N_5O^+$: 306.1349; found: 307.1387 (14), 306.1349 (100) $[M+H]^+$.

4-{2-[(Cyclopentylmethyl)amino]ethyl}-2-(methylamino)-1,7-dihydro-8*H*-imidazo[4,5-*g*]quinazolin-8-one (10a): According to GP 1, starting from **9a** (58 mg, 0.13 mmol) in anhydrous formamide (4.0 mL). The crude product was directly used according to GP 2a to yield **10a** (26 mg, 60% over two steps) as a white foam. M.p. >315 °C (decomp); ^{1}H NMR (600 MHz, $(CD_3)_2SO$): δ=1.23 (dt, *J*=13.3, 7.6 Hz, 2H; H–C(2′,5′)), 1.46–1.54 (m, 2H; H–C(3′,4′)), 1.57–1.62 (m, 2H; H–C(3′,4′)), 1.77 (dt, *J*=13.3, 7.1 Hz, 2H; H–C(2′,5′)), 2.16 (q, *J*=7.5 Hz, 1H; H–C(1′)), 2.93 (d, *J*=7.2 Hz, 2H; CH_2–C(1′)), 2.96 (s, 3H; NMe), 3.17 (t, *J*=7.1 Hz, 2H; CH_2–C(4)), 3.54 (t, *J*=7.1 Hz, 2H; CH_2CH_2–C(4)), 7.60 (br s, 1H; NH), 7.70 (s, 1H; H–C(9)), 7.95 (s, 1H; H–C(6)), 8.39 ppm (s, 2H; 2NH); ^{13}C NMR (150 MHz, $(CD_3)_2SO$): δ=23.27 (CH_2–C(4)), 25.08 (2C; C(3′,4′)), 29.40 (NMe), 30.62 (2C; C(2′,5′)), 37.27 (C(1′)), 47.67 (CH_2–C(1′)), 52.14 (CH_2CH_2–C(4)), 104.62 (C(4)), 115.86 (C(9)), 116.33 (C(8a)), 138.09 (C(3a)), 141.65 (C(9a)), 145.75 (C(4a)), 160.03 (C(6)), 161.90 (C(2)), 165.97 ppm (C(8)); IR (ATR): $\tilde{\nu}$=3352 (m), 3143 (m), 3016 (m), 2911 (m), 2869 (m), 2803 (m), 1699 (s), 1664 (s), 1600 (s), 1449 (s), 1291 (m), 1226 (m), 1190 (m), 1158 (m), 1097 (m), 1023 (m), 984 (m), 896 (m), 826 (m), 802 (m), 760 (m), 689 cm^{-1} (m); HR-MALDI-MS: *m*/*z*: calcd (%) for $C_{18}H_{25}N_6O^+$: 341.2084; found: 342.2129 (13), 341.2088 (100) $[M+H]^+$.

4-{2-[(Cyclohexylmethyl)amino]ethyl}-2-(methylamino)-1,7-dihydro-8*H*-imidazo[4,5-*g*]quinazolin-8-one (10b): According to GP 1, starting from **9b** (70 mg, 0.15 mmol) in anhydrous formamide (4.0 mL). The crude product was directly used according to GP 2a to yield **10b** (35 mg, 66%) as a white foam. M.p. >298 °C (decomp); ^{1}H NMR (600 MHz, $(CD_3)_2SO$): δ=0.93 (qd, *J*=11.9, 2.4 Hz, 2H; H_{ax}–C(2′,6′)), 1.12 (tt, *J*=12.3, 3.2 Hz, 1H; H_{ax}–C(4′)), 1.16–1.24 (m, 2H; H_{ax}–C(3′,5′)), 1.60–1.70 (m, 4H; H–C(1′), H_{eq}–C(2′,3′,5′)), 1.75 (br d, *J*=13.2 Hz, 2H; H_{eq}–C(2′,6′)), 2.79 (d, *J*=6.8 Hz, 2H; CH_2–C(1′)), 2.96 (s, 3H; NMe), 3.13 (t, *J*=7.3 Hz, 2H; CH_2–C(4)), 3.51 (t, *J*=7.3 Hz, 2H; CH_2CH_2–C(4)), 7.60 (br s, 1H; NH), 7.69 (s, 1H; H–C(9)), 7.94 (s, 1H; H–C(6)), 8.42 ppm (s, 2H; NH); ^{13}C NMR (150 MHz, $(CD_3)_2SO$): δ=22.92 (CH_2–C(4)), 25.02 (2C; C(3′,5′)), 25.61 (NMe), 28.82 (C(4′)), 30.05 (2C;

C(2′,6′)), 34.85 (C(1′)), 47.39 (CH_2–C(1′)), 52.83 (CH_2CH_2–C(4)), 104.04 (C(9)), 115.31 (C(4)), 116.00 (C(8a)), 137.30 (C(3a)), 141.00 (C(9a)), 144.68 (C(4a)), 159.44 (C(6)), 161.33 (C(2)), 165.53 ppm (C(8)); IR (ATR): $\tilde{\nu}$ = 3366 (m), 3008 (m), 2924 (m), 2853 (m), 2808 (m), 1689 (s), 1661 (s), 1598 (s), 1445 (s), 1291 (m), 1225 (m), 1188 (w), 1157 (w), 1102 (w), 983 (m), 889 (m), 843 (m), 762 (m), 689 cm^{-1} (m); HR-MALDI-MS: *m*/*z*: calcd (%) for $C_{19}H_{27}N_6O^+$: 355.2241; found: 356.2283 (23), 355.2247 (100) $[M+H]^+$.

2,6-Bis(methylamino)-1,7-dihydro-8*H*-imidazo[4,5-*g*]quinazolin-8-one (11a): According to GP 2a, starting from **18a** (49 mg, 0.109 mmol) and yielding **11a** (23 mg, 87%) as a white solid. M.p. >304 °C (decomp); ^{1}H NMR (600 MHz, $(CD_3)_2SO$): δ = 2.82 (d, *J* = 4.2 Hz, 3H; NMe), 2.89 (d, *J* = 3.0 Hz, 3H; NMe), 6.29 (br s, 1H; NH), 6.82 (br s, 1H; NH), 6.91 (s, 1H; H–C(4)), 7.55 ppm (s, 1H; H–C(9)); ^{13}C NMR (150 MHz, $(CD_3)_2SO$): δ = 27.39 (NMe), 28.87 (NMe), 104.95 (C(9)), 110.16 (C(4)), 145.70 (2C; C(3a,9a)), 150.25 (C(2)), 158.52 (C(6)), 163.65 (2C; C(4a,8a)), 166.84 ppm (C(8)); IR (ATR): $\tilde{\nu}$ = 3253 (w, sh), 3042 (w), 2932 (w), 1682 (m), 1672 (m), 1597 (s), 1570 (m), 1536 (m), 1450 (m), 1411 (s), 1350 (m), 1330 (m), 1283 (m), 1227 (m), 1207 (m), 1152 (m), 1118 (m), 979 (m), 871 (m), 864 (m), 782 (m), 627 cm^{-1} (m); HR-MALDI-MS: *m*/*z*: calcd (%) for $C_{11}H_{12}N_6NaO^+$: 267.0970; found: 267.0970 (99) $[M+Na]^+$; *m*/*z*: calcd (%) for $C_{11}H_{13}N_6O^+$: 245.1145; found 245.1151 (100) $[M+H]^+$.

6-(Ethylamino)-2-(methylamino)-1,7-dihydro-8*H*-imidazo[4,5-*g*]quinazolin-8-one (11b): According to GP 2a, starting from **18b** (124 mg, 0.266 mmol) and yielding **11b** (59 mg, 86%) as a white solid. M.p. >269 °C (decomp); ^{1}H NMR (300 MHz, 1 M aqueous NaOD solution): δ = 1.07 (t, *J* = 7.7 Hz, 3H; NCH_2CH_3), 2.82 (s, 3H; NMe), 3.22 (q, *J* = 7.7 Hz, 2H; NCH_2CH_3), 6.95 (s, 1H; H–C(4)), 7.54 ppm (s, 1H; H–C(9)); ^{13}C NMR (150 MHz, $(CD_3)_2SO$): δ = 14.84 (NCH_2CH_3), 28.95 (NMe), 34.96 (CH_2CH_3), 105.20 (C(9)), 110.18 (C(4)), 145.85 (2C; C(3a,9a)), 149.10 (C(2)), 158.66 (C(6)), 163.38 (2C; C(4a,8a)), 167.32 ppm (C(8)); IR (ATR): $\tilde{\nu}$ = 3448 (w), 3249 (w, sh), 3103 (w, sh), 3030 (w), 2973 (w), 2920 (w), 2878 (w), 1672 (w), 1592 (s), 1567 (m), 1515 (m), 1472 (m), 1432 (m), 1409 (s), 1365 (m), 1340 (m), 1321 (m), 1282 (m), 1228 (m), 1186 (m), 1164 (m), 1123 (m), 1106 (m), 1017 (w), 982 (w), 858 (m), 844 (m), 780 (m), 679 (m), 657 (m), 621 cm^{-1} (m); HR-MALDI-MS: *m*/*z*: calcd (%) for $C_{12}H_{14}N_6NaO^+$: 281.1127; found: 281.1118 (87) $[M+Na]^+$; *m*/*z*: calcd (%) for $C_{12}H_{15}N_6O^+$: 259.1302; found: 259.1298 (100) $[M+H]^+$.

***Z. mobilis* TGT crystallization**: Protein was cloned, overexpressed, and purified as described in detail elsewhere.[34] Crystals of TGT appropriate for data collection were obtained by using the hanging-drop, vapor-diffusion method at 288 K. TGT was cocrystallized with inhibitors. A protein solution (12 mg mL^{-1} TGT, 10 mM Tris-HCl (Tris = tris(hydroxymethyl)-aminomethane), pH 7.8, 2 M NaCl, 1 mM EDTA (ethylenediaminetetraacetic acid), 15% (v/v) Me_2SO) was incubated with 1.5 mM inhibitor. A total of 2 μL of this solution was mixed with 2 μL reservoir solution (100 mM MES (2-(N-morpholino)ethanesulfonic acid), pH 5.5, 1 mM DTT (dithiothreitol), 10% (v/v) Me_2SO, 13% (w/v) polyethylene glycol (PEG) 8000). After three weeks of crystal growth, crystals reached dimensions around $0.7 \times 0.7 \times 0.2$ mm^3. Instead of cocrystallization, compounds **8b**,**c** were soaked at a final concentration of 5 mM for one day into wild-type crystals.

X-ray data collection: Crystals were transferred for 10 s into a cryoprotectant-containing buffer (50 mM MES, pH 5.5, 300 mM NaCl, 0.5 mM DTT, 2% (v/v) Me_2SO, 4% (w/v) PEG 8000, 30% (v/v) glycerol). Afterwards, crystals were flash-frozen in liquid nitrogen. All datasets were collected under cryo conditions (100 K) at the BESSY-PSF Beamline 14.2 in Berlin at a wavelength of λ = 0.91841 Å. A Rayonix MX225 CCD detector was used for data collection. TGT crystals exhibited a monoclinic space group *C*2 with one monomer per asymmetric unit. Data processing and scaling was carried out using HKL2000. Unit-cell dimensions, data collection, and processing statistics are given in Table 2.

Structure determination and refinement: For all complexes, the CNS program package was used to perform the initial rigid-body refinement and a cycle of conjugate gradient energy minimization, simulated annealing, and B-factor refinement.[35] The coordinates of the TGT apo structure 1P0D were used as starting model. Due to the high resolution of all datasets, further refinement using SHELXL-97 was performed.[36] For each refinement step, at least 20 cycles of conjugate gradient minimization were made with default restraints on bond lengths, angles, and *B* values. A total of 5% of all data were used for R_{free} calculation. Intermittent model building was performed using COOT.[37] The ligand, water, and glycerol molecules were placed into the sigma-A weighted difference electron density and included in further refinement cycles. Riding hydrogen atoms were added for the protein in a final refinement cycle without using additional parameters. Model analysis was performed using PROCHECK.[38] Coordinate files were deposited in the PDB with the following access codes: 3S1G, 3GEV, 3V0Y, 3SM0, 3RR4, 3TLL.

Acknowledgements

We are grateful to the ETH Research Council, F. Hoffmann-La Roche (Basel), and Chugai Pharmaceuticals for the generous support of the work done at ETH. The research at the University of Marburg was supported by a grant from the Deutsche Forschungsgesellschaft (KL1204/13-1). We thank Daniel Zimmerli (Roche, Basel) for advice regarding HPLC, Dr. Bruno Bernet (ETH) for proofreading the Experimental Section, Michael Seet (ETH) for proofreading the manuscript, and Pablo Rivera-Fuentes (ETH) for DFT calculations. We acknowledge the support from the beamline staff at BESSY II in Berlin and a travel grant from the Helmholtz-Zentrum für Materialien und Energie in Berlin.

[1] C. Frank, M. S. Faber, M. Askar, H. Bernard, A. Fruth, A. Gilsdorf, M. Höhle, H. Karch, G. Krause, R. Prager, A. Spode, K. Stark, D. Werber, *Euro. Surveill.* **2011**, *16*, pii = 19878. Available online: http://www.eurosurveillance.org/ViewArticle.aspx?ArticleId = 19878.

[2] P. J. Sansonetti, *FEMS Microbiol. Rev.* **2001**, *25*, 3–14.

[3] J. M. B. Durand, B. Dagberg, B. E. Uhlin, G. R. Björk, *Mol. Microbiol.* **2000**, *35*, 924–935.

[4] U. Grädler, H.-D. Gerber, D. M. Goodenough-Lashua, G. A. Garcia, R. Ficner, K. Reuter, M. T. Stubbs, G. Klebe, *J. Mol. Biol.* **2001**, *306*, 455–467.

[5] B. Stengl, E. A. Meyer, A. Heine, R. Brenk, F. Diederich, G. Klebe, *J. Mol. Biol.* **2007**, *370*, 492–511.

[6] E. A. Meyer, N. Donati, M. Guillot, W. B. Schweizer, F. Diederich, B. Stengl, R. Brenk, K. Reuter, G. Klebe, *Helv. Chim. Acta* **2006**, *89*, 573–597.

[7] For an overview, see: a) N. J. Leonard, A. G. Morrice, M. A. Sprecker, *J. Org. Chem.* **1975**, *40*, 356–363; b) G. E. Keyser, N. J. Leonard, *J. Org. Chem.* **1976**, *41*, 3529–3532; c) N. J. Leonard, F. Kaźmierczak, A. Rykowski, *J. Org. Chem.* **1987**, *52*, 2933–2935.

[8] For *lin*-benzoadenine-based inhibitors of the *S*-adenosyl-L-homocysteine (SAH) hydrolase, see: a) H. Dvořáková, A. Holý, M. Masojídková, *Collect. Czech. Chem. Commun.* **1988**, *53*, 1779–1794; b) V. P. Rajappan, S. W. Schneller, *Tetrahedron* **2001**, *57*, 9049–9053.

[9] For *lin*-benzoadenine-based inhibitors of the epidermal growth factor receptor (EGFR), see: a) G. W. Rewcastle, B. D. Palmer, A. J. Bridges, H. D. H. Showalter, L. Sun, J. Nelson, A. McMichael, A. J. Kraker, D. W. Fry, W. A. Denny, *J. Med. Chem.* **1996**, *39*, 918–928; b) Y. B. Lee, C. H. Ahn, Patent US 2005/0187231A1, **2005**.

[10] For 6-arylimidazo[4,5-*g*]quinazolin-8(7*H*)-ones as inhibitors of phosphodiesterase type 5 (PDE5), see: a) J. E. Macor, D. P. Rotella, H. N. Weller, III, D. W. Cushman, J. P. Yevich, Patent US 6087368, **2000**; b) D. P. Rotella, Z. Sun, Y. Zhu, J. Krupinski, R. Pongrac, L. Seliger, D. Normandin, J. E. Macor, *J. Med. Chem.* **2000**, *43*, 5037–5043.

[11] For an overview, see: a) H. Liu, J. Gao, L. Maynard, Y. D. Saito, E. T. Kool, *J. Am. Chem. Soc.* **2004**, *126*, 1102–1109; b) H. Liu, S. R. Lynch, E. T. Kool, *J. Am. Chem. Soc.* **2004**, *126*, 6900–6905; c) J. Gao, H. Liu, E. T. Kool, *J. Am. Chem. Soc.* **2004**, *126*, 11826–11831; d) H. Liu, J. Gao, E. T. Kool, *J. Org. Chem.* **2005**, *70*, 639–647; e) A. R. Hernández, E. T. Kool, *Org. Lett.* **2011**, *13*, 676–679;

f) A. T. Krueger, L. W. Peterson, J. Chelliserry, D. J. Kleinbaum, E. T. Kool, *J. Am. Chem. Soc.* **2011**, *133*, 18447–18451.
[12] S. R. Hörtner, T. Ritschel, B. Stengl, C. Kramer, W. B. Schweizer, B. Wagner, M. Kansy, G. Klebe, F. Diederich, *Angew. Chem.* **2007**, *119*, 8414–8417; *Angew. Chem. Int. Ed.* **2007**, *46*, 8266–8269.
[13] P. C. Kohler, T. Ritschel, W. B. Schweizer, G. Klebe, F. Diederich, *Chem. Eur. J.* **2009**, *15*, 10809–10817.
[14] T. Ritschel, P. C. Kohler, A. Heine, F. Diederich, G. Klebe, *ChemMedChem* **2009**, *4*, 2012–2023.
[15] For some examples on the preference for guanine-based over hypoxanthine-based ligands, see: a) R. Seifert, U. Gether, K. Wenzel-Seifert, B. K. Kobilka, *Mol. Pharmacol.* **1999**, *56*, 348–358; b) M. J. Barnes, N. Cooper, R. J. Davenport, H. J. Dyke, F. P. Galleway, F. C. A. Galvin, L. Gowers, A. F. Haughan, C. Lowe, J. W. G. Meissner, J. G. Montana, T. Morgan, C. L. Picken, R. J. Watson, *Bioorg. Med. Chem. Lett.* **2001**, *11*, 1081–1083; c) S. Kohgo, K. Yamada, K. Kitano, Y. Iwai, S. Sakata, N. Ashida, H. Hayakawa, D. Nameki, E. Kodama, M. Matsuoka, H. Mitsuya, H. Ohrui, *Nucleosides Nucleotides Nucleic Acids* **2004**, *23*, 671–690; d) A. B. Eldrup, C. R. Allerson, C. F. Bennett, S. Bera, B. Bhat, N. Bhat, M. R. Bosserman, J. Brooks, C. Burlein, S. S. Caroll, P. D. Cook, K. L. Getty, M. MacCoss, D. R. McMasters, D. B. Olsen, T. P. Prakash, M. Prhavc, Q. Song, J. E. Tomassini, J. Xia, *J. Med. Chem.* **2004**, *47*, 2283–2295.
[16] For some examples on the preference for hypoxanthine-based over guanine-based ligands, see: a) Q. Chao, L. Deng, H. Shih, L. M. Leoni, D. Genini, D. A. Carson, H. B. Cottam, *J. Med. Chem.* **1999**, *42*, 3860–3873; b) Y. Chong, H. Choo, Y. Choi, J. Mathew, R. F. Schinazi, C. K. Chu, *J. Med. Chem.* **2002**, *45*, 4888–4898; c) M. Bretner, S. Schalinski, P. Borowski, T. Kulikowski, *Nucleosides Nucleotides Nucleic Acids* **2003**, *22*, 1531–1533.
[17] For some examples of PNP inhibitors, see: a) S. Niwas, P. Chand, V. P. Pathak, J. A. Montgomery, *J. Med. Chem.* **1994**, *37*, 2477–2480; b) P. E. Morris, Jr., A. J. Elliott, S. P. Walton, C. H. Williams, J. A. Montgomery, *Nucleosides Nucleotides Nucleic Acids* **2000**, *19*, 379–404; c) E. A. Taylor, K. Clinch, P. M. Kelly, L. Li, G. B. Evans, P. C. Tyler, V. L. Schramm, *J. Am. Chem. Soc.* **2007**, *129*, 6984–6985.
[18] W. Xie, X. Liu, R. H. Huang, *Nat. Struct. Biol.* **2003**, *10*, 781–788.
[19] G. M. Coppola, G. E. Hardtmann, O. R. Pfister, *J. Org. Chem.* **1976**, *41*, 825–831.
[20] N. Pluym, A. Brennauer, M. Keller, R. Ziemek, N. Pop, G. Bernhardt, A. Buschauer, *ChemMedChem* **2011**, *6*, 1727–1738.
[21] T. Ritschel, S. Hörtner, A. Heine, F. Diederich, G. Klebe, *ChemBioChem* **2009**, *10*, 716–727.
[22] A. Leo, C. Hansch, D. Elkins, *Chem. Rev.* **1971**, *71*, 525–616.
[23] *ACD/Labs*, Version 12.01, Advanced Chemistry Development, Inc., Toronto, **2009**.
[24] For reviews of PAMPA scores, see: a) S. Bendels, O. Tsinman, B. Wagner, D. Lipp, I. Parrilla, M. Kansy, A. Avdeef, *Pharm. Res.* **2006**, *23*, 2525–2535; b) A. Avdeef, S. Bendels, L. Di, B. Faller, M. Kansy, K. Sugano, Y. Yamauchi, *J. Pharm. Sci.* **2007**, *96*, 2893–2909.
[25] X. Gong, M. Figus, J. Plewa, D. A. Levorse, L. Zhou, C. J. Welch, *Chromatographia* **2008**, *68*, 219–225.
[26] B. Stengl, K. Reuter, G. Klebe, *ChemBioChem* **2005**, *6*, 1926–1939.
[27] R. Brenk, M. T. Stubbs, A. Heine, K. Reuter, G. Klebe, *ChemBioChem* **2003**, *4*, 1066–1077.
[28] For reviews on water clusters, see: a) J. E. Ladbury, *Chem. Biol.* **1996**, *3*, 973–980; b) R. Ludwig, *Angew. Chem.* **2001**, *113*, 1856–1876; *Angew. Chem. Int. Ed.* **2001**, *40*, 1808–1827; c) S. W. Homans, *Drug Discovery Today* **2007**, *12*, 534–539; d) P. Ball, *Chem. Rev.* **2008**, *108*, 74–108.
[29] T. Petrova, H. Steuber, I. Hazemann, A. Cousido-Siah, A. Mitschler, R. Chung, M. Oka, G. Klebe, O. El-Kabbani, A. Joachimiak, A. Podjarny, *J. Med. Chem.* **2005**, *48*, 5659–5665.
[30] A. Biela, F. Sielaff, F. Terwesten, A. Heine, T. Steinmetzer, G. Klebe, *J. Med. Chem.* DOI: 10.1021/jm300337q.
[31] H. Steuber, A. Heine, G. Klebe, *J. Mol. Biol.* **2007**, *368*, 618–638.
[32] M. Ellermann, R. Jakob-Roetne, C. Lerner, E. Borroni, D. Schlatter, D. Roth, A. Ehler, M. G. Rudolph, F. Diederich, *Angew. Chem.* **2009**, *121*, 9256–9260; *Angew. Chem. Int. Ed.* **2009**, *48*, 9092–9096.
[33] *The PyMOL Molecular Graphics System*, Version 1.3; Schrödinger, Inc., New York, **2010**.
[34] For a detailed description of *Z. mobilis* TGT crystallization, see: a) C. Romier, R. Ficner, K. Reuter, D. Suck, *Proteins* **1996**, *24*, 516–519; b) C. Romier, K. Reuter, D. Suck, R. Ficner, *EMBO J.* **1996**, *15*, 2850–2857; c) K. Reuter, R. Ficner, *J. Bacteriol.* **1995**, *177*, 5284–5288.
[35] A. T. Brünger, P. D. Adams, G. M. Clore, W. L. DeLano, P. Gros, R. W. Grosse-Kunstleve, J.-S. Jiang, J. Kuszewski, M. Nigles, N. S. Pannu, R. J. Read, L. M. Rice, T. Simonson, G. L. Warren, *Acta Crystallogr. Sect. D* **1998**, *54*, 905–921.
[36] G. M. Sheldrick, T. R. Schneider, *Methods Enzymol.* **1997**, *277*, 319–343.
[37] P. Emsley, K. Cowtan, *Acta Crystallogr. Sect. D* **2004**, *60*, 2126–2132.
[38] R. A. Laskowski, *J. Appl. Crystallogr.* **1993**, *26*, 283–291.

Received: March 10, 2012
Published online: ■■ ■■, 0000

Water replacements: A series of *lin*-benzopurines was evaluated as inhibitors of *Zymomonas mobilis* tRNA–guanine transglycosylase, an enzyme that was identified as a potential target for the treatment of shigellosis. X-ray cocrystal structures show the import of a new water cluster that replaces lost protein–ligand interactions (see figure), with an overall reduction in binding affinity.

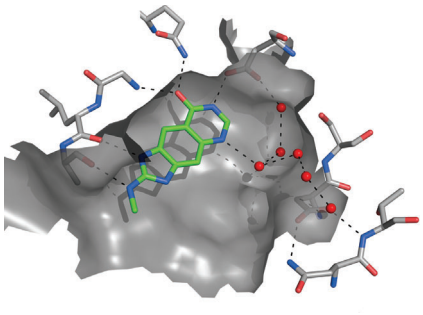

Drug Design

L. J. Barandun, F. Immekus, P. C. Kohler, S. Tonazzi, B. Wagner, S. Wendelspiess, T. Ritschel, A. Heine, M. Kansy, G. Klebe, F. Diederich** ..... ▮▮▮▮–▮▮▮▮

From *lin*-Benzoguanines to *lin*-Benzohypoxanthines as Ligands for *Zymomonas mobilis* tRNA–Guanine Transglycosylase: Replacement of Protein–Ligand Hydrogen Bonding by Importing Water Clusters